Flexible 2.4 GHz Node for Body Area Networks with a Compact High-Gain Planar Antenna

Mahmoud Wagih, Yang Wei, and Steve Beeby, *Senior Member* IEEE

***Abstract*— A flexible 2.4 GHz wireless sensor node with a bespoke single layer monopole antenna, tuned for on-body operation for wearable applications, is presented. Multiple antenna design approaches for tuning on-body antennas have been investigated. The proposed antennas, patch and meandered, designed for operation in the insole, exhibit a simulated realised gain of -3.98 dB and -1.97 dB respectively. The antennas were fabricated on a 25 µm flexible polyimide substrate, exhibiting up to 16% lower insertion losses at 20 GHz than FR4 PCBs. The integrated node incorporates a commercial Bluetooth Low Energy (BLE) system-on-chip and exhibits 9 dB higher measured gain than commercial modules with reference antenna design. Moreover, through functional radio test, it was confirmed that the designed node passes Bluetooth transmitter certification tests.**

***Index Terms*—Flexible Antenna, Smart Textiles, Human-Proximity Effects, Body Area Networks (BAN), Internet of Things**

I. Introduction

Advances in electronics fabrication have enabled the production of flexible circuits on fabric and polymer substrates for wearable applications. For example, antennas [1, 2], sensors [3] and energy harvesters [4] have been demonstrated on flexible polymer or fabric-based circuits. Nevertheless, novel flexible antenna designs were never integrated in flexible wireless transmitters and tested for functionality, as well as compliance with the chosen wireless protocol standards.

Polyimide (i.e. Kapton) copper laminates, have been widely used in fabricating flexible printed-circuits (FPCs) due to their high flexibility and dielectric characteristics [1, 5]. Compared to inkjet printed circuits, they cater for improved reliability and heat-tolerance; allowing utilisation of existing PCB assembly and fabrication facilities.

Flexible antennas in the Industrial Scientific Medical (ISM) band are commonly tested for robustness against bending [6]. Moreover, body area networks (BAN) [7], and body-implantable antennas [8], operating at 2.4 GHz, were previously presented. For instance, Mendes *et al.* presented a dual-mode antenna with separate feedlines for on and off-body operation [7]. Jung *et al.* presented radiator length variation as a tuning method for body-plantar antennas [9]. The flexible antennas were fabricated by etching polyimide copper laminates [9], or 3D and inkjet printing of the conductor where the antenna's efficiency is adversely reduced due to the material's conductivity [10].

Only the work by Krykpayev *et al.* and Mihajlovic *et al.* demonstrates wireless transmitters realised on a flexible substrate [11, 12]. However, the utilisation of reference antenna designs makes the nodes susceptible to detuning by human proximity [13]. In this letter, an integrated flexible node, with bespoke antenna design, tuned for on-body operation is presented. Moreover, implications of different on-body antenna tuning paradigms have been investigated and evaluated.

II. Antennas Design

Three antenna designs were proposed and further tuned through simulation, each aiming to achieve optimal on-body performance using a different design approach, as discussed in section V. Firstly, a meandered inverted-F, initially designed as a quarter-wavelength monopole, with a total radiator length of 3.1 cm meandered for compactness and reducing the fringing capacitance with the ground plane; for improved efficiency in human proximity. The antenna is tuned to resonate at 2.4 GHz in foot by changing the radiator length to the dimensions in figure 1. A single layer patch has been designed based on design-aid formulae, with a ground shorting line on the same layer, and resized post simulation to account for the human-proximity effect observed through simulation.

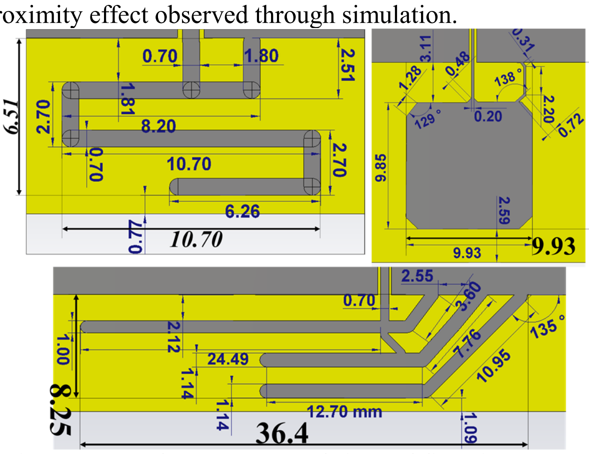

Figure 1. Proposed 2.4 GHz antenna designs and dimensions (mm). Clock-wise from top-left: Meandered PIFA, Patch and Dual-arm PIFA.

A dual arm planar inverted-F antenna (PIFA), with an additional director arm, inspired by the Yagi antenna, has been designed based on simulation results of inverted-F antennas.

This work was supported by the European Commission through the project EnABLES: European Infrastructure Powering the Internet of Things, funded under H2020-EU.1.4.1.2 and the Engineering and Physical Sciences Research Council through the project Novel Manufacturing Methods for Functional Electronic Textiles under Grant EPSRC EP/M015149/1.

M. Wagih, Y. Wei and S. Beeby are with the Smart Electronic Materials and Systems Research Group, in the Department of Electronics and Computer Science, University of Southampton, Southampton, UK, SO17 1BJ (email: mahm1g15@ecs.soton.ac.uk, yw1f10@ecs.soton.ac.uk, spb@ecs.soton.ac.uk).

Data published in this paper are available from the University of Southampton repository at 10.5258/SOTON/D0702.

The dual radiators aim to increase the bandwidth around 2.4 GHz and hence reduce susceptibility to detuning.

A reference PIFA from Texas Instruments with 3.3 dBi gain [14], widely utilised in research and industry [11], has been simulated and fabricated for benchmarking. The designs were tuned for a 25 µm thick Polyimide substrate with 12 µm copper, and a 12 µm epoxy adhesive layer.

III. Flexible Circuit Design and Fabrication

Although polyimide has been widely adopted in the FPCs industry, an investigation of the insertion losses through simulation and measurements has been performed for verifying the high-speed performance. As the design is aimed at a single layer fabrication process, the only viable transmission line structure is a coplanar waveguide (CPW). Given the conductor thickness, the closest achievable impedance to 50 Ω was 83 Ω; due to the natively low capacitance of the structure. The gap width was not reduced bellow 150 µm to match commercial board houses design-rules, the line width was capped at 800 µm to match the size of 0603 passive components' pads.

The CPW has been simulated in CST Microwave Studio (CST), a 3D high frequency simulator. Lossy polyimide and lossy copper models were used for the CPW model. Furthermore, as skin depth losses are significantly affected by the surface roughness [15], the roughness of the copper laminates was set to 1 µm. Figure 2 shows the simulated forward transmission of Polyimide and FR4 12 cm long CPW, verified through measurements, up to 4 GHz, of the fabricated CPW sample, showing lower losses by up to 16% at 20 GHz.

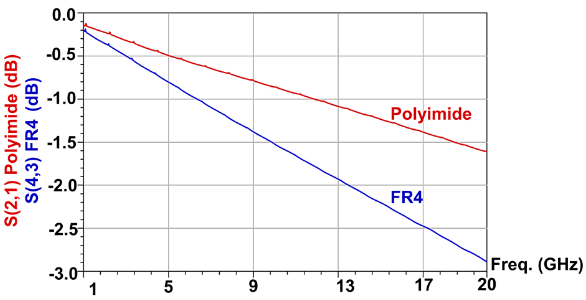

Figure 2. Forward transmission through a 12cm long CPW on Polyimide, s(2,1) and FR4, s(4,3), substrate, showing 16% lower insertion losses on Polyimide compared to FR4 at 20 GHz.

The FPC has been fabricated using standard photolithography techniques commonly used in PCBs fabrication. A photomask has been used for UV decomposition of a photosensitive ink layer prior to etching the copper using a commercial copper etcher. Figure 3 shows the fabricated circuit before and after copper etching. The selected 2.4 GHz wireless System on Chip (SoC) is Texas Instruments' CC2640R2F, supporting the latest Bluetooth as well as Bluetooth Low Energy (BLE) version. The FPC's layout compromises the CC2640R2F BLE SoC, associated crystal oscillators and decoupling capacitors, RF filtering, a 1st order matching network and the proposed antennas. A power management circuit, based on Linear's LTC3588, is also included to allow powering the system from energy harvesting sources. Figure 4 shows the populated flexible sensor node.

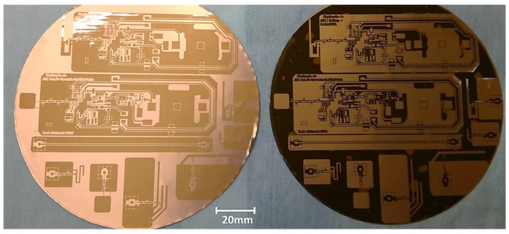

Figure 3. Fabricated flexible circuit housing two system designs and antennas samples, before (left) and after (right) copper etching.

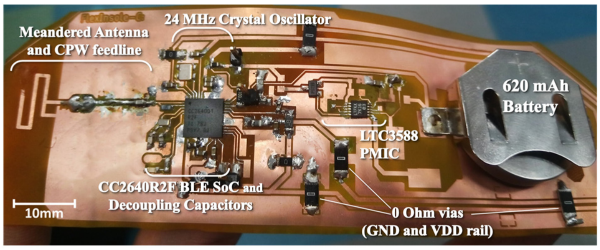

Figure 4. Populated flexible wireless sensor node with the proposed meandered antenna, showing the key system components.

IV. Antennas Simulation and Measurements

The proposed antennas were simulated in CST, using the time-domain solver for improved mesh accuracy. As a wireless wearable device is most susceptible to detuning and absorption when placed in the insole, a simplified model of a human foot, using CST's Voxel library [16], was designed to model a foot-plantar device. The separation between the foot and the antennas was initially set to 1 mm and tuned to 0.5 mm and 3 mm in the insole and in human-proximity respectively, to reach the maximum accuracy of the simulated S_{11} and the radiation patterns, based on the S_{11} measurements of the meandered antenna. CPW feed, of 2.2 cm length, was included to observe its impact on the input impedance of the antenna. An Electric-field boundary condition has been enforced under the infinitely-wide soil layer; to disregard the radiation into the earth. The 3D model of the antenna in foot is shown in figure 5.

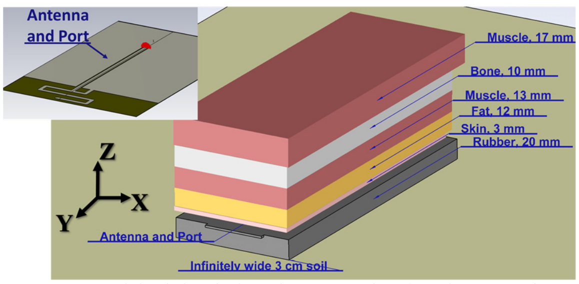

Figure 5. CST model of the designed antenna showing the user's foot, shoe insole and soil, excited by a 50Ω discrete port.

The fabricated antenna samples include a CPW feed of 2.5 cm length. The antenna under test (AUT) was measured using a Rhode and Schwarz ZVB4 Vector Network Analyser (VNA) and fed using a 50Ω SMA port. The AUTs were measured in two test conditions: free space, and on-body: where the antenna is placed at 5 mm beneath the user's forearm with a layer of fabric as separation. An additional foot-plantar test, were the AUT is placed underneath the user's foot and above a rubber shoe insole, was performed with the meandered antenna, after tuning it by shortening the radiator length. Figures 6-8 show the simulated and measured return losses. The resonance shifting towards lower frequencies in human-proximity is due to the increase in the antenna's capacitance, thus the meandered antenna has been tuned by reducing the radiator length, as discussed in section V.

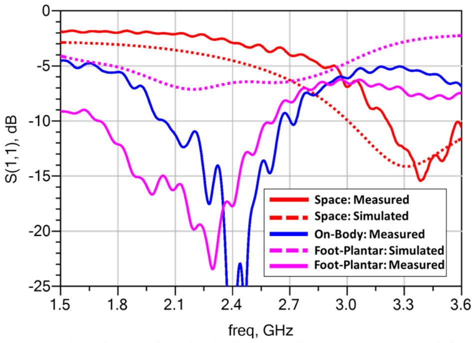

Figure 6. Measured and simulated (dashed) reflection, s(1,1), of the meandered antenna in space, human contact and in foot, showing ultrawide band in human-contact and in foot.

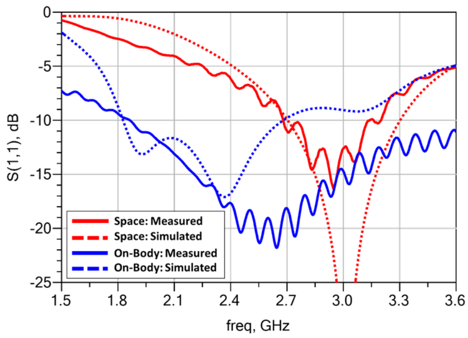

Figure 7. Measured and simulated (dashed) reflection, s(1,1), of the patch antenna in space and in foot, showing < -6dB reflection under all test conditions.

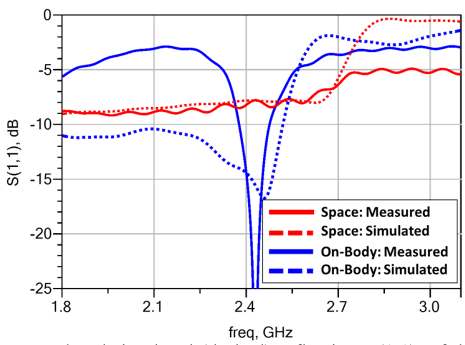

Figure 8. Measured and simulated (dashed) reflection, s(1,1), of the dual-arm PIFA in space and in human-proximity, showing ultra-wide bandwidth in space due to the dual radiator and resonance at 2.4 GHz in human-proximity.

CST field monitors were used to measure the near and far-fields of the antennas, in addition to the power losses and the specific absorption rate (SAR), normalised at 10 gm. Figure 9 show the simulated farfield radiation patterns of the proposed antennas in free space as well as in a foot-planar device. Table 1 shows the characteristics of each antenna.

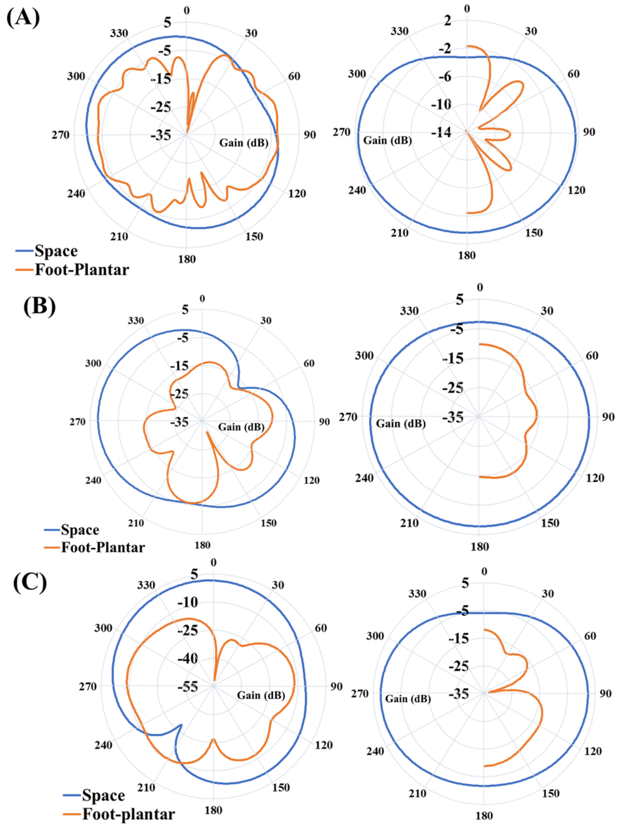

Figure 9. Simulated antennas radiation patterns (A: Meandered, B: Patch and C: Dual-arm PIFA), in space and in foot, on the *xy*-plane (left) and *xz*-plane (right), showing lower gain on the vertical *xz*-plane due to absorption.

TABLE I
SIMULATED ANTENNA CHARACTERISTICS (2.42 GHZ)

Antenna	Gain in Space (dB)	Gain in foot (dB)	Realised Gain, in foot (dB)	Max. SAR in foot (W/kg)	Board Area (cm^2)
Patch	2.29	-3.85	-3.96	19.4	1.44
Meandered	1.96	-0.87	-1.97	15.1	0.78
Dual ARM PIFA	2.71	-7.04	-10.85	17.5	3.33
TI Reference PIFA [14]	2.3	-11.77	-13.13	20.5	2.02

V. BODY PROXIMITY EFFECTS

The antenna's impedance can be simplified into inductance and capacitance, where the capacitance is composed of the parallel plate capacitance between the side edges of the radiator arm and the ground plane, in addition to the fringing capacitance between the planes' top surfaces; due to the electric field above the antenna, where the dielectric properties of the surroundings significantly affect the fringing and hence the overall capacitance. The proposed meandered and patch antenna demonstrate minimal horizontal length and therefore the fringing capacitance between the radiator and the ground plane is minimised compared to conventional inverted-F antennas, this can be verified by observing the simulated electric field magnitude on top of the antennas, shown in figure 10. The additional capacitance introduced by the higher dielectric constant of human tissue, compared to air, is less significant due to the minimised fringing capacitance. To add, the reduced electric field reduces the overall SAR of the proposed meandered antenna compared to the proposed patch and reference PIFA.

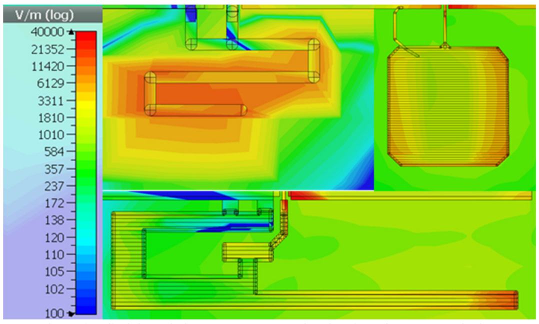

Figure 10. Electric fields of the antennas (clockwise from top-left: Meandered, Patch and reference PIFA) showing higher electric field between the PIFA's arm and the ground plane compared to the proposed designs, resulting in higher fringing capacitance and susceptibility to detuning.

The human proximity detuning effect can be overcome by tuning the antenna through varying the radiator length, this has been utilised in tuning the designed meandered antenna and in Jung's study [9]. The proposed patch is a single-mode antenna, aiming to operate both on and off-body, for maximum design portability. Antennas specifically designed for body-plantar applications, such as the proposed dual-arm PIFA and Kim *et al*. PIFA present superior on-body impedance match, to single-mode antennas (proposed patch), with poor-performance off-body performance. Mendes *et al.* antenna demonstrates high gain on-body, however, the antenna has been kept at 4 mm above the body model [7]; implying lower impact on the far-field and on the antenna reactive field at 2.4 GHz. Table 2 shows a comparison of the antennas' characteristics variation based on the design tuning methodology. The lower gain of the proposed antenna is due to the absorption by the 5 cm-thick human foot inside the antenna's reactive field.

TABLE II
ON-BODY ANTENNAS COMPARISON

Antenna: On-body Tuning Methodology	Resonance in Space (GHz)	Return Loss in Space (dB)	Resonance on Body (GHz)	Return Loss on Body (dB)	Gain on Body (dB)
Patch: Single mode	2.8	-15.2	2.6	-20	-3.96*
Meandered: Length reduction	3.4	-15.4	2.4	-49	-1.97*
Dual-arm PIFA: Empirical, 3D Simulation	1.8 to 2.6	-8.4	2.44	-45	-10.9*
Mendes *et al* [7]: Dual mode	2.4	-20.5	2.458	-17	4.1‡
Jung *et al.* [9]: Length variation	0.7	-22	2.4	-18	0.8†
Kim *et al.* [13]	0.470	-2.5	0.443	-7	-0.1†

* CST Simulated realised gain † Reported body-plantar measured gain
‡ Reported measured gain at 4 mm from body phantom

VI. RF FRONTEND TESTING

A. Link Budget Measurements

Broadband link budget measurement of the AUTs was performed using the VNA, where the AUT is connected to port 1 and an omnidirectional 2.4 GHz antenna is connected to port 2; to quantify the link budget at 50 cm distance, in the main lobe direction. Figure 12 shows the link budget of the proposed meandered antenna and the reference PIFA; demonstrating 9 dB and 3.5 dB higher transmitter gain in foot and in space respectively, compared to the reference at 2.4 GHz, on the Polyimide substrate.

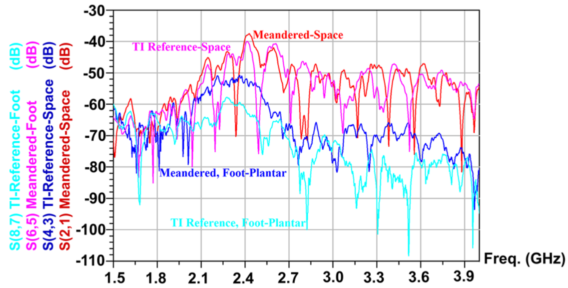

Figure 11. Measured Link budget of the meandered antenna, s(2,1) and s(4,3), and the reference PIFA, s(6,5) and s(8,7), in space and in foot; showing improved gain of the proposed antenna compared to the reference by up to 9 dB in foot.

B. Bluetooth Transmitter Test

The transmitter test defined in the Bluetooth certification standards has been replicated using a spectrum analyser connected to a 50Ω input. The BLE SoC was configured to transmit continuously at 2 dBm, the maximum specified output by the manufacturer, in the 2.402 GHz channel. Figure 12 shows the measured received power passing the -20 dBm test threshold, with -10.4 dBm measured at 2.402 GHz. The transmitted power test has been repeated using TI's reference wireless module in space and human-proximity, where the flexible transmitter showed equal performance in space and 14 dB higher transmitter gain in human proximity.

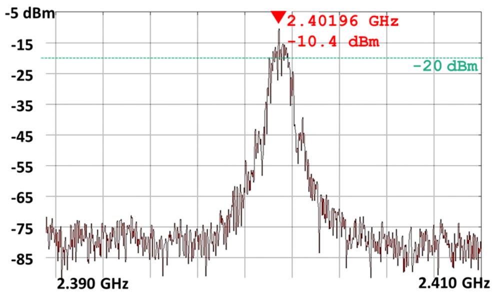

Figure 12. Received power test, using a spectrum analyser, showing transmitter power complying with Bluetooth transmitter certification standard.

VII. CONCLUSION

A 2.4 GHz node, for BANs, materialised on a low-cost flexible substrate with a bespoke compact antenna, tuned for on-body operation by radiator length shortening, has been presented. Multiple methodologies for designing high-gain on-body antenna were compared with factors reducing antennas' susceptibility to detuning identified and exploited. The proposed compact meandered antenna exhibits 1.96 dB and -1.97 dB simulated realised gain in space and in the insole respectively. The demonstrated node surpasses an industrial reference antenna design by 9 dB measured gain, in the insole, and is potentially compliant with Bluetooth transmitter standards.

REFERENCES

[1] S.-E. Adami, P. Proynov, G. S. Hilton, G. Yang, C. Zhang, D. Zhu, Y. Li, S. P. Beeby, I. J. Craddock and B. H. Stark, "A Flexible 2.45-GHz Power Harvesting Wristband With Net System Output From −24.3 dBm of RF Power," *IEEE Transactions on Microwave Theory and Techniques ,* vol. 66, no. 1, pp. 380-395, 2018.

[2] W. G. Whittow, A. Chauraya, J. C. Vardaxoglou, Y. Li, R. Torah, K. Yang, S. Beeby and J. Tudor, "Inkjet-Printed Microstrip Patch Antennas Realized on Textile for Wearable Applications," *IEEE Antennas and Wireless Propagation Letters,* vol. 13, pp. 71 - 74, 2014.

[3] G. M. Paul, F. Cao, R. Torah, K. Yang, S. Beeby and J. Tudor, "A Smart Textile Based Facial EMG and EOG Computer Interface," *IEEE Sensors Journal,* vol. 14, no. 2, pp. 393 - 400, 2013.

[4] Z. Luo, Z. D., J. Shi, S. Beeby, C. Zhang, P. Proynov and B. Stark, "Energy Harvesting Study on Single and Multilayer Ferroelectret Foams under Compressive Force," *IEEE Transactions on Dielectrics and Electrical Insulation ,* vol. 22, no. 3, pp. 1360-1369, 2015.

[5] S. Kiya, K. Morizane, Y. Uchita and M. Kouchi, "Thin Flexible Printed Circuit Supporting Transmission Rate from 1 to 10 Gbps," *SEI TECHNICAL REVIEW,* vol. 80, pp. 12-16, 2015.

[6] A. Tronquo, H. Rogier, C. Hertleer and L. V. Langenhove, "Robust planar textile antenna for wireless body LANs operating in 2.45 GHz ISM band," *Electronics Letters ,* vol. 42, no. 3, pp. 142 - 143, 2006.

[7] C. Mendes and C. Peixeiro, "A Dual-Mode Single-Band Wearable Microstrip Antenna for Body Area Networks," *IEEE Antennas and Wireless Propagation Letters,* vol. 16, pp. 3055 - 3058, 2017.

[8] M. L. Scarpello, D. Kurup, H. Rogier, D. V. Ginste, F. Axisa, J. Vanfleteren, W. Joseph, L. Martens and G. Vermeeren, "Design of an Implantable Slot Dipole Conformal Flexible Antenna for Biomedical Applications," *IEEE Transactions on Antennas and Propagation,* vol. 59, no. 10, pp. 3556 - 3564, 2011.

[9] Y. H. Jung, Y. Qiu, S. Lee, T.-Y. Shih, Y. Xu, R. Xu, J. Lee, A. A. Schendel, W. Lin, J. C. Williams, N. Behdad and Z. Ma, "A Compact Parylene-Coated WLAN Flexible Antenna for Implantable Electronics," *IEEE Antennas and Wireless Propagation Letters,* vol. 15, pp. 1382 - 1385, 2015.

[10] M. Rizwan, M. W. A. Khan, L. Sydänheimo, J. Virkki and L. Ukkonen, "Flexible and Stretchable Brush-Painted Wearable Antenna on a Three-Dimensional (3-D) Printed Substrate," *IEEE Antennas and Wireless Propagation Letters,* vol. 16, pp. 3108 - 3112, 2017.

[11] B. Krykpayev, M. F. Farooqui, R. M. Bilal and A. Shamim, "A WiFi tracking device printed directly on textile for wearable electronics applications," in *IEEE Microwave Symposium (IMS)*, San Francisco, CA, USA, 2016.

[12] Ž. Mihajlović, V. Milosavljević, D. Vasiljević, A. Joža, V. Rajs and M. Živanov, "Implementation of wearable energy harvesting wireless sensor node using ink-jet printing on flexible substrate," in *5th Mediterranean Conference on Embedded Computing*, Montenegro, 2016.

[13] J. Kim and Y. Rahmat-Samii, "Implanted antennas inside a human body: simulations, designs, and characterizations," *IEEE Transactions on Microwave Theory and Techniques ,* vol. 52, no. 8, pp. 1934 - 1943, 2004.

[14] Texas Instruments, "2.4-GHz Inverted F Antenna," April 2007. [Online]. Available: http://www.ti.com/lit/an/swru120c/swru120c.pdf. [Accessed 2017].

[15] M. D. Rotaru and M. A. Wagih, "Analysis and design of low loss differential transmission line structures for high speed applications," in *IEEE 19th Electronics Packaging Technology Conference (EPTC)*, Singapore, 2017.

[16] Y. H. a. Q. X. Rula Alrawashdeh, "Evaluation of Implantable Antennas in Anatomical Body Models," [Online]. Available: https://www.cst.com/solutions/article/evaluation-of-implantable-antennas-in-anatomical-body-models.